LIVERPOOL JOHN MOORES UNIVERSITY

LJMU Research Online

Zhang, JF, Ji, Z and Zhang, WEI

As-grown-Generation (AG) Model of NBTI: a shift from fitting test data to prediction

http://researchonline.ljmu.ac.uk/id/eprint/7616/

Article

Citation (please note it is advisable to refer to the publisher's version if you intend to cite from this work)

Zhang, JF, Ji, Z and Zhang, WEI (2017) As-grown-Generation (AG) Model of NBTI: a shift from fitting test data to prediction. Microelectronics Reliability. ISSN 0026-2714

LJMU has developed **LJMU Research Online** for users to access the research output of the University more effectively. Copyright © and Moral Rights for the papers on this site are retained by the individual authors and/or other copyright owners. Users may download and/or print one copy of any article(s) in LJMU Research Online to facilitate their private study or for non-commercial research. You may not engage in further distribution of the material or use it for any profit-making activities or any commercial gain.

The version presented here may differ from the published version or from the version of the record. Please see the repository URL above for details on accessing the published version and note that access may require a subscription.

For more information please contact researchonline@ljmu.ac.uk

http://researchonline.ljmu.ac.uk/

As-grown-Generation (AG) Model of NBTI: a shift from fitting test data to prediction

J. F. Zhang, Z. Ji, and W. Zhang

Department of Electronics and Electrical Engineering, Liverpool John Moores University
Byrom Street, Liverpool, L3 3AF, UK

Abstract

Negative bias temperature instabilities (NBTI) received little attention pre-2000, but have been intensively investigated post-2000, as they become limiting device lifetime. The relatively thick oxides and low electrical field used in the pre-2000 works make hole injection into oxides negligible. In contrast, hole injection is substantial for most of the post-2000 research that used thin oxides and high fields. This leads to a number of discrepancies between pre- and post-2000 works, in terms of kinetics, recovery, and relative contribution of different types of defects. To account for these discrepancies, a number of models have been proposed. Although these models can fit accelerated test data well, evidences are not enough to convince that they can predict the long term NBTI under low use-Vdd. This article first reviews the discrepancies between pre- and post-2000 works and then uses the Reaction-Diffusion framework as an example to show its inability of prediction for general processes. Evidences for the presence of both As-grown Hole Traps (AHTs) and Generated Defects (GDs) during typical NBTI stresses are presented and techniques for their separation are described. This lays the foundation for the As-grown-Generation (AG) model and its prediction capability will be demonstrated, followed by an analysis why AG model can predict, while others cannot. Finally, speculations are made on the mechanism, defects, and damaging species in terms of holes, hydrogenous species, and their interactions. Although atomic structures of defects are not known, some conditions for their candidates are given.

1. Introduction

Only four years after CMOS technology was invented, negative bias temperature instability (NBTI) was reported in 1967 [1], making it one of the earliest instabilities identified for CMOS. In the following three decades or so, NBTI received little attention [2-4], as it was not the limiting mechanism for device lifetime. Towards the end of last century, however, NBTI has been limiting the device lifetime, as shown in Fig. 1 [5]. This has motivated extensive research on NBTI since 2000 [6-20]. NBTI research can be conveniently divided into two groups: pre- and post-2000.

Pre-2000, most of works on NBTI were carried out on thick (i.e. typically >5 nm) SiO_2 or SiON under relatively low oxide fields (i.e. typically < 7MV/cm) [1-4]. This combination of thick oxides and low fields makes hole injection into oxides insignificant during stress and the NBTI reported pre-2000 has several signatures:

- There is a one-to-one correlation between the generation of interface states and the formation of oxide charges [1-3], as reported by the first paper on NBTI in Fig. 2 [1].
- Recovery after removing the negative gate bias is modest, i.e. substantially less than half of the total degradation [1].
- NBTI kinetics follows a power law with a time exponent typically of 0.25 [2,4]. This power law was explained by hydrogen diffusion through oxides as the rate limiting process [2]. It allows predicting long term NBTI by extrapolating the power law, as illustrated in Fig. 3 [21].

Post-2000 NBTI works [6-20], however, often do not clearly exhibit these signatures and the new models proposed will be described in Section 2. Although all models can fit test data well, there are not enough evidences confirming that they can predict long term NBTI under low use-Vdd for different CMOS processes. We will use the reaction-diffusion (RD) model as an example to show that it cannot make the required prediction. Section 3 will introduce the As-grown-Generation (AG) model and show that it can predict. The concept of defect generation will be discussed and clear evidence will be given to support the separation of As-grown Hole Traps (AHTs) from the Generated Defects (GDs). The reasons for the success of AG models are analyzed. Section 4 gives some speculations on defects and damaging species, including holes, hydrogenous species, and their interactions. Finally, Section 5 summarizes the paper.

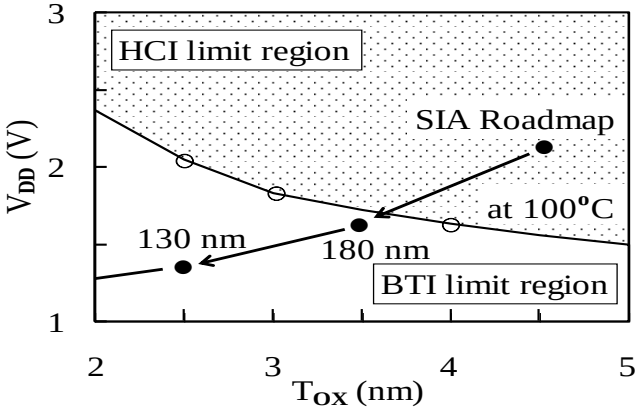

Fig. 1. NBTI becomes a lifetime limiting mechanism post-2000. [5].

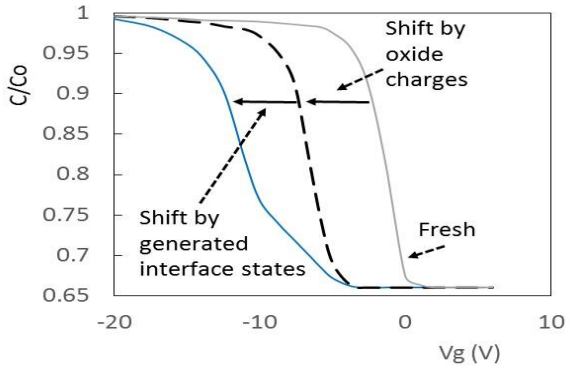

Fig. 2. One-to-one correlation between the oxide charges and the generated interface states. [1].

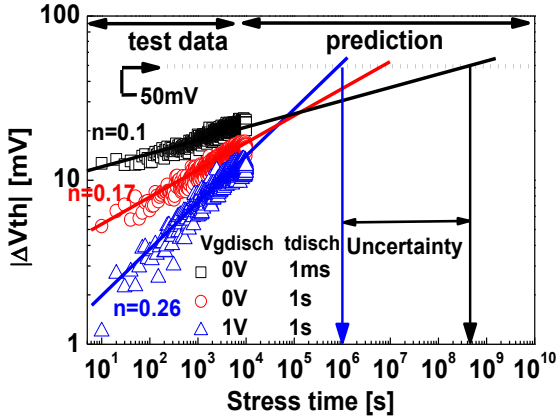

Fig. 3. An example of NBTI prediction by extrapolation and the uncertainty induced by the different time exponents obtained after different measurement delays. [21].

2. Post-2000 models

2.1. Differences between pre- and post-2000 NBTI works

The signatures in pre-2000 NBTI often cannot be clearly observed in many of post-2000 works:

- There is generally no one-to-one correlation between the generation of interface states and the formation of oxide charges. The oxide charges can recover much faster than interface states, so that the ratio of oxide charges against interface states depends on the measurement delay after stress [19]. When the recovery was minimized by using pulse measurement with a delay in the order of micro-seconds, oxide charges are generally higher than the generated interface states [19] and their ratio is also process dependent [13,23].
- Recovery after removing stress bias can be substantially higher than half of the total degradation. For example, Fig. 4 shows that recovery can be over 80% [22]. An increase of nitrogen concentration in SiON enhances the recovery [13,23].
- NBTI kinetics no longer follows a simple power law against stress time, especially when measured by the pulse IV technique [7, 12, 24]. A 'hump' is often observed in the early stage of stress and one example is given in Fig. 5 [24].

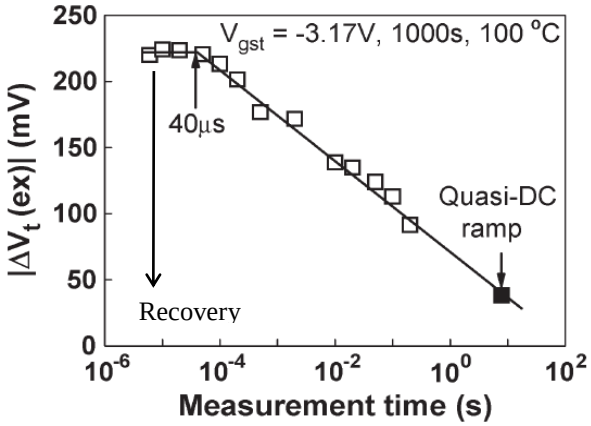

Fig. 4. Recovery of NBTI can be well over 50% for thin oxides used in post-2000 works. [22].

2.2. Restore the power law by measurement delay

When pulse measurement with a delay in the order of microseconds was used, the 'hump' behavior in Fig. 5 makes it problematic to predict long term NBTI through the extrapolation illustrated in Fig. 3. To facilitate the prediction through such an extrapolation, power law has to be restored. One method for doing this is to introduce a measurement delay [24-26]. The defects responsible for the 'Hump' recovers faster, so that it can be suppressed by using a sufficient delay between stress and measurement, as shown in Fig. 6 [24]. The problem is that Fig. 3 shows the time exponent changes with the delay time, making the accuracy of prediction based on a particular delay questionable [21].

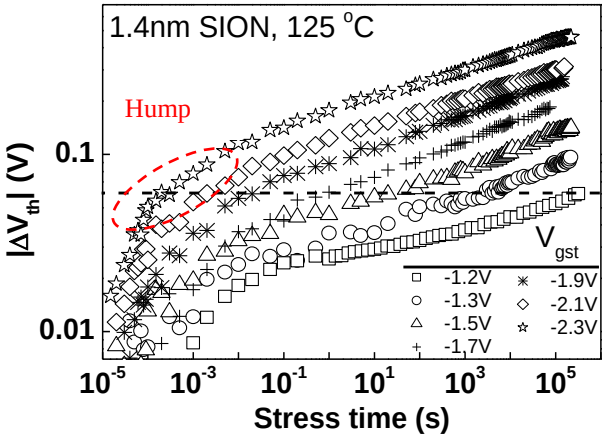

Fig. 5. NBTI by pulse measurements does not follow a power law well. [24].

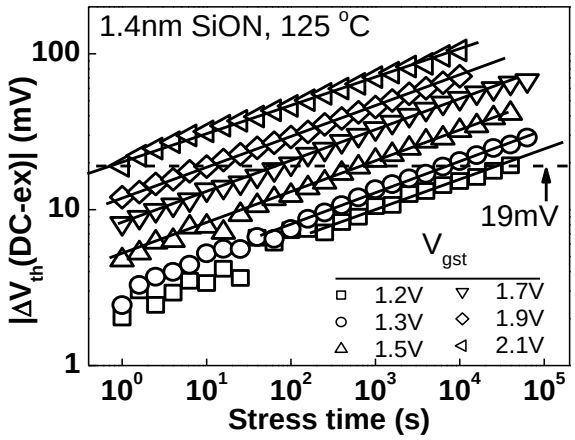

Fig. 6. Power law can be restored by adding a measurement delay. The wafer used here is the same as that in Fig. 5. [24].

2.3. Modelling post-2000 non-power law NBTI

To do better than using a delay to restore the power law, a number of models were developed for the non-power law NBTI kinetics, including various versions of Reaction-Diffusion (RD) model [6,7], the composite model [13,14], and the capture-emission time mapping model [10,11].

The capture-emission time mapping model uses different capture and emission times for different traps in oxides [8,11]. The composite model divides total degradation into two components: recoverable and 'permanent' [13,14]. Power law is applied only to permanent component, while recoverable component increases linearly against logarithmic stress time. The RD based framework [7] divides degradation into three groups of defects: interface states, pre-existing hole traps, and new hole traps. Power law is applied only to the generation of interface states with a fixed time exponent of 1/6, which is believed to originate from the diffusion of H_2 through oxides [6,7].

All these models can fit test data well. The mission for NBTI modelling, however, is to predict long term NBTI beyond practical test time under low use-Vdd, based on the model extracted from short accelerated stresses. There are not enough evidences confirming that these models can deliver the required prediction. In the following, we will use the RD framework [7] as an example to show that it generally cannot deliver the required prediction for different processes.

The test samples fabricated by four different processes are summarized in Table I, covering a wide range of fabrication techniques and dielectrics. Their NBTI are given in Fig. 7. The processes D1 and D2 are high-k stacks and D2 has the highest NBTI, representing a process under development. D3 is a mature plasma nitrided SiON with the lowest NBTI among the four processes. D4 is a thermally nitrided SiON, used to represent the case for samples with a high density of As-grown Hole Traps (AHTs) [23].

For all four processes, accelerated short DC stresses were carried out under different constant over-drive voltages at 125 °C and the results are given in the upper-panels of Figs. 8(a)-(d). The threshold voltage shift, ΔVth, was monitored from Vg shift at a constant sensing Id= 100 nA×W/L by pulse IV with an edge time of 3 μs [27].

Device number	Gate dielectrics	EOT
D1	HfO2 with TiN gate	1.45nm
D2	HfSiON/SiON with TiN gate	1.53nm
D3	Plasma SiON with high N% and P+ poly gate	2.0nm
D4	Thermal SiON with poly gate	2.7nm

TABLE I Samples used in this work

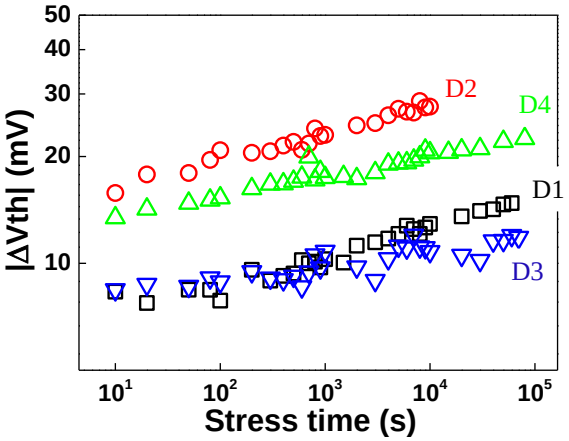

Fig. 7. NBTI aging of the four samples listed in Table I under the Vg=-1.1 V at 125 °C.

The upper-panels of Figs. 8(a)-(d) show that RD framework can fit test data well in all cases. The extracted model parameters were then used to predict the NBTI under low bias over longer stress period, as presented by the lines in the lower panels of Figs. 8(a)-(d). To test the accuracy of prediction, NBTI under these low biases is also measured and given as symbols in the lower panels and these test data were not used for extracting model parameters. It is clear that the prediction by RD framework generally does not agree with test data and can be either higher or lower than test data.

One may question whether the poor agreement in Fig. 8 results from incorrect implementation of the RD model. To verify the implementation, we used our program to fit the test data from ref. 6 and obtained the same parameter values as those reported in ref. 6

3. As-grown-Generation (AG) model

Since early models generally cannot predict long term NBTI under low use-Vdd, the original mission of NBTI modelling has not been achieved. The As-grown-Generation (AG) model [28,29] has been proposed recently to deliver the required prediction capability.

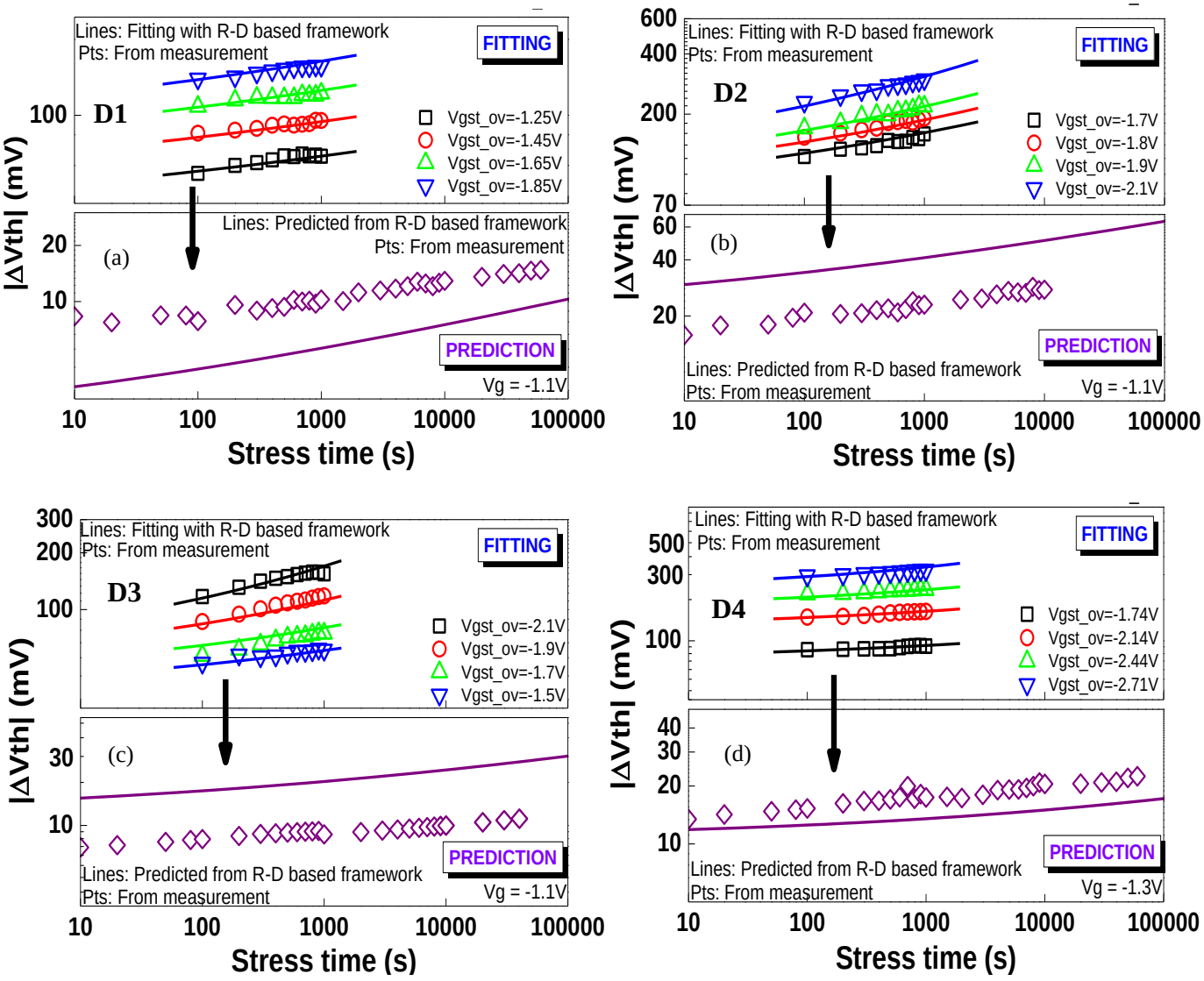

Fig. 8. The upper panels of (a)-(d) for the four processes in Table I give the ΔVth measured from short accelerated stresses and the lines are fitted with the RD framework. The extracted model was then used to predict ΔVth under low operating Vg in the lower panels. The prediction (lines) does not agree with the test data (symbols).

The AG model divides defects into two groups: As-grown Hole Traps (AHTs) that pre-exist in fresh devices and Generated Defects (GDs), where precursors have to go through a conversion process when charged for the first time.

To lay the foundation for AG model, we first review the concepts of AHTs and GDs in Sections 3.1 and 3.2, respectively. A framework for the stress-induced positive charges in oxides will be given in Section 3.3, supported by their energy profiles. Section 3.4 describes techniques for separating GDs from AHTs and Section 3.5 demonstrates the prediction capability of AG model, based on the same test data where RD framework failed to predict. Section 3.6 discuss the reasons why AG model can predict.

3.1. As-Grown Traps

The classical and simplest trapping kinetics assume that a trap has an effective physical size, called capture cross section, σ [30-33]. A carrier coming cross this area in its path will be captured. This first order trapping kinetics gives,

$$N = Ns\left(1 - e^{-\frac{t}{\tau}}\right), \qquad (1)$$

where N is the number of filled traps per unit area, Ns is the saturation level of N. t is stress time and the characteristic capture time, τ, is,

$$\tau = \frac{q}{J\sigma}, \qquad (2)$$

where J is injection current per unit area and q one electron charge. As time constant, τ, depends on test conditions through J, we prefer using capture cross section, σ, which is a fundamental trap property. A different version of eq. (1) is [33],

$$N = Ns\left(1 - e^{-\frac{\sigma Q}{q}}\right), \qquad (3)$$

where the charge fluency Q is,

$$Q = \int_0^t J\, dt\,. \qquad (4)$$

A feature of this kinetics is that it will saturate: N reaches over 98% of Ns at t=4τ and filling lasts one and half order of Q approximately, as illustrated by the two vertical dashed lines for σ_2 in Fig. 9. The problem is that such clear saturation is rarely observed experimentally and Fig. 9 shows that test data typically do not fit well with a single σ. The lack of saturation has puzzled the community and different explanations have been given: multiple or a spread of σ [31-33]; interaction of traps [34]; and generation of new defects [35,36].

If traps can have multiple capture cross sections, eq. (3) is modified to,

$$N = \sum_{i=1}^{M} N_{Si}\left(1 - e^{-\frac{\sigma_i Q}{q}}\right), \qquad (5)$$

where M is the number of capture cross sections.

The spatial location of traps is typically not known and a common practice is to assume that they are at the oxide/Si interface and the corresponding 'effective density' is related to the threshold voltage shift, ΔVth, by [35],

$$N = \frac{Cox \times \Delta Vth}{q}. \qquad (6)$$

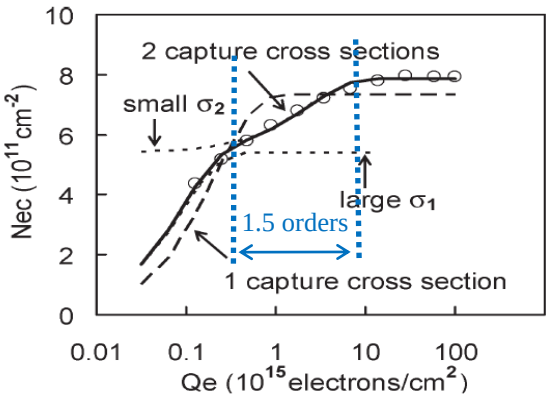

Fig. 9. Single capture cross section covers one and half orders of magnitude (see the double-arrowed blue line) and multiple capture cross sections often are needed to fit the test data. [31]

As-grown Hole Traps indeed can have more than one capture cross sections and one example is given in Fig. 10 [37], where filling AHTs lasts three orders of magnitude of charge fluency approximately. As filling traps of a given capture cross section only takes one and half orders in Fig. 9, the AHT-filling in Fig. 10 cannot be fitted with just one capture cross section.

The reservation of many researchers for introducing multiple capture cross sections is that by using a large number of capture cross sections, one can fit any test data. It is not clear whether a good agreement with test data achieved in this way is simply a 'curve-fitting' [31-35]. As a result, care must be exercised and ideally, justification should be sought each time a new capture cross section is added.

The data in Fig. 10 can be fitted in two possible ways: by using a continuous distribution of capture cross sections or by introducing a discrete second capture cross section. The former suggests a gradual and continuous change of σ and trap properties/structures, while the latter indicates an abrupt change, possibly by the presence of a different type of AHTs. If it is a gradual change, one would expect that the impact of processing also will be gradual. On the other hand, if there are two different types of defects for AHTs, they can have different dependence on processing. Fig. 10 clearly shows that the larger traps, controlling trapping at low Q_{inj}, are hardly affected by the processing, while the smaller traps, responsible for trapping at high Q_{inj}, are sensitive to it. This abrupt change in process dependence supports the presence of two discrete σ.

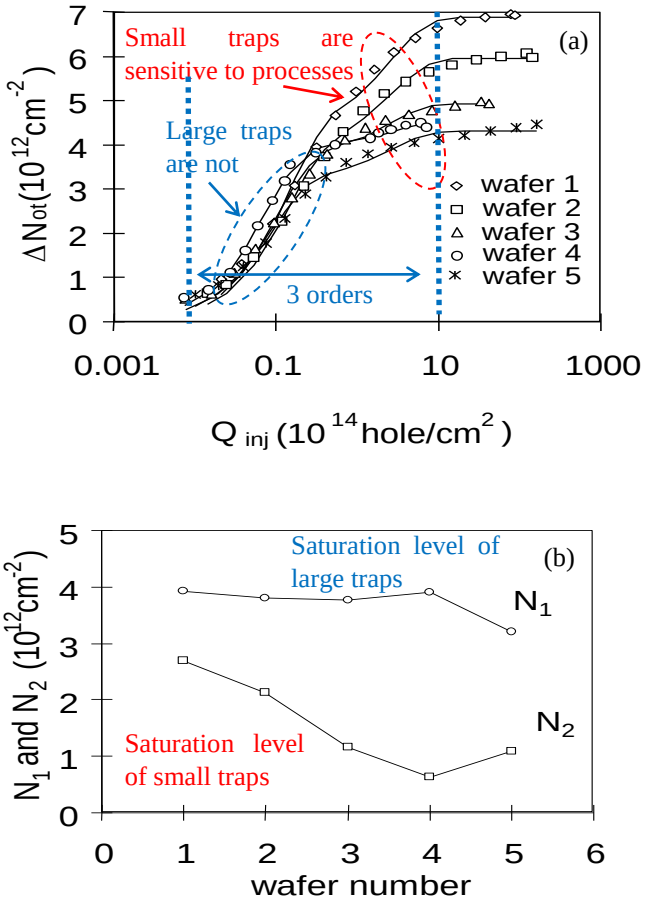

Fig. 10. Justification of the presence of two capture cross sections: (a) The larger one is not sensitive to process conditions, while the small one is. (b) is the fitted saturation levels. [37].

On trap interaction, it was proposed that after capturing a charge, a trap can reduce the probability for traps nearby to be filled through Coulombic repulsion [34]. Although this explanation is physically appealing, Fig. 10 shows that trapping up to $7x10^{12}$ q/cm^2 can be modelled well without taking the

interaction into account. A typical device lifetime defined as ΔVth=50 mV corresponds to an effective charge density of $7x10^{11}$ q/cm^2 for a 1.5 nm equivalent oxide thickness. As a result, interaction among traps is not significant within a device lifetime. Next, we will show that non-saturation of charging is often a signature of trap generation, rather than filling traps of smaller capture cross sections.

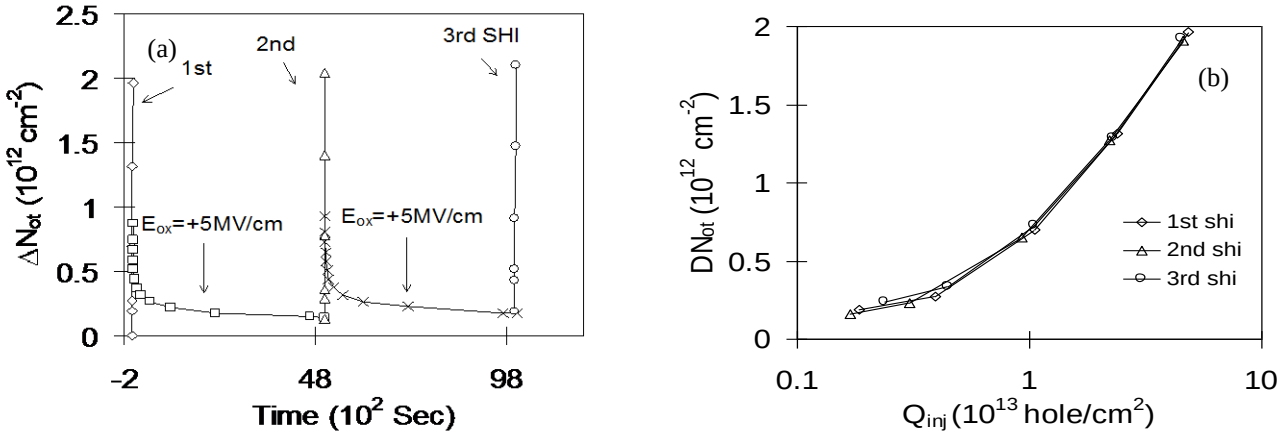

Fig. 11. Before trap generation at low stress levels (a), the same trapping during the refilling occurs as that of the first filling (b). [35].

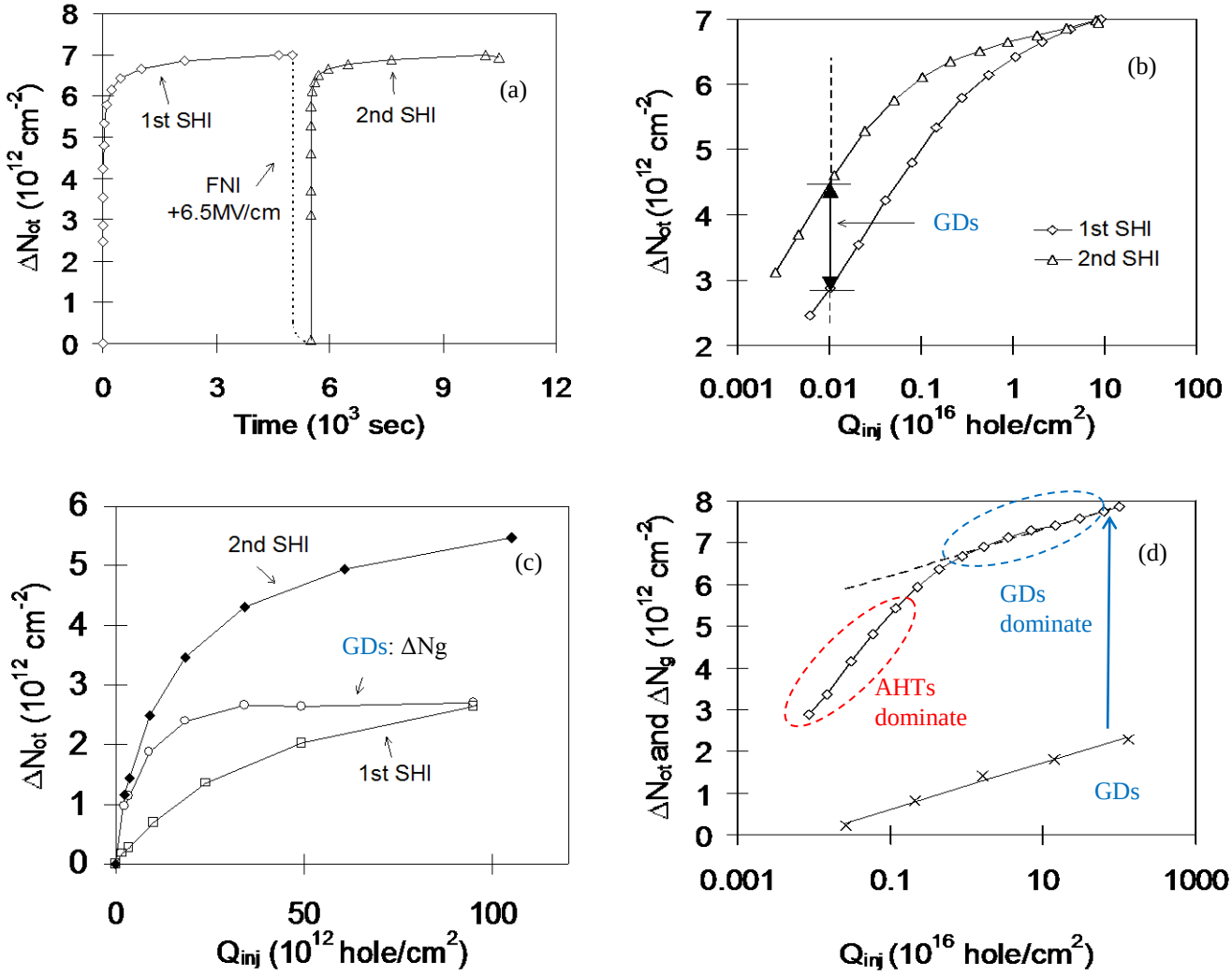

Fig. 12. After high level stress (a), refilling is higher than the first filling, due to the newly generated defects (GDs) (b). (c) shows that filling GDs, ΔNg, is rapid and follows the first-order model. (d) shows GDs controlling the positive charge build-up at high stress level. [35].

3.2. Hole trap generation

The term 'generation' was used for an increase of interface states during the hot carrier stress initially [38]. It was used later for the time dependent dielectric breakdown (TDDB), where generated defects formed a percolation path through oxides, triggering the breakdown [39,40]. A stress-induced leakage current (SILC) generally precedes breakdown and has been used as a measure of defect generation [40]. It is important, however, to point out that some generated defects contribute little to SILC/breakdown [41], so that 'no SILC' does not necessarily mean 'no generation'. The defects for SILC/Breakdown act as step-stones for carriers through rapid capture-emission and they may not form stable charging [42]. As a result, SILC and IV can probe different defects. Before we address generated hole traps, we need a clear definition for them against as-grown ones.

As-grown traps are the traps that, following filling-detrapping, their subsequent filling efficiency will not increase and their energy levels remains the same. Fig. 11(a) shows the cycling of low level of hole injection/trapping-neutralization and Fig. 11(b) shows that the refilling follows the same kinetics/capture cross sections as the first filling. This confirms that there are no new traps available for filling after the short stress during the first filling.

In contrast, generated traps can be defined as the traps whose other properties, in addition to charge status, have been changed pre- or during capturing a carrier for the first time. In another word, there is a generation process that converts a precursor into a trap that can then be filled effectively.

Fig. 12(a) shows the cycling of heavy hole injection -neutralization and Fig. 12(b) shows that the refilling is clearly higher than the 1st filling initially [35]. There are more hole traps with large capture cross sections after a heavy stress, therefore. By definition, these are 'generated' hole traps. To show it clearly, Fig. 12(c) plots the difference between the 2nd and 1st filling. Importantly, this difference, ΔNg, saturates quickly and can be modelled well with a single capture cross section [35], supporting that, once a trap is created, the filling process itself is fast.

The insignificant difference at the end of two fillings in Fig. 12(b) can also be explained. During the 1st heavy stress, traps are generated and then promptly filled. As the generation follows a power law, the additional generation during the 2nd stress is insignificant when compared with that of the 1st stress for the same stress time, so that trapping reaches similar levels at the end of two fillings.

Fig. 12(d) compares the amount of generated hole traps with the trapping kinetics at heavy stress level. The excellent agreement supports that the non-saturation of hole trapping at high stress level during the 1st stress originates from the relatively slow generation process. The same data could be fitted well by using a number of smaller capture cross sections, which would be an artefact.

3.3. A framework for positive charges in oxides and their energy profile

A framework for positive charges in oxides is proposed, based on their charge-discharge properties, as illustrated in Fig. 13(a) [43,44]. In addition to AHTs, the generated hole traps were divided into Cyclic Positive Charges (CPCs) and Anti-Neutralization Positive Charges (ANPCs).

After filling all three types of traps during stress on a 5.5 nm SiON, they were completely neutralized by applying a positive oxide field, Eox, of +8 MV/cm. An Eox=-5 MV/cm was then applied during which the generated hole traps were recharged, while AHTs were not. When gate bias polarity was alternated, some GDs can be repeatedly discharged under +5 MV/cm and recharged under -5 MV/cm. They are referred to as Cyclic Positive Charges (CPCs). At the end of discharge period under +5 MV/cm, some GDs are not be neutralized, so that they are called as Anti-Neutralization Positive Charges (ANPCs).

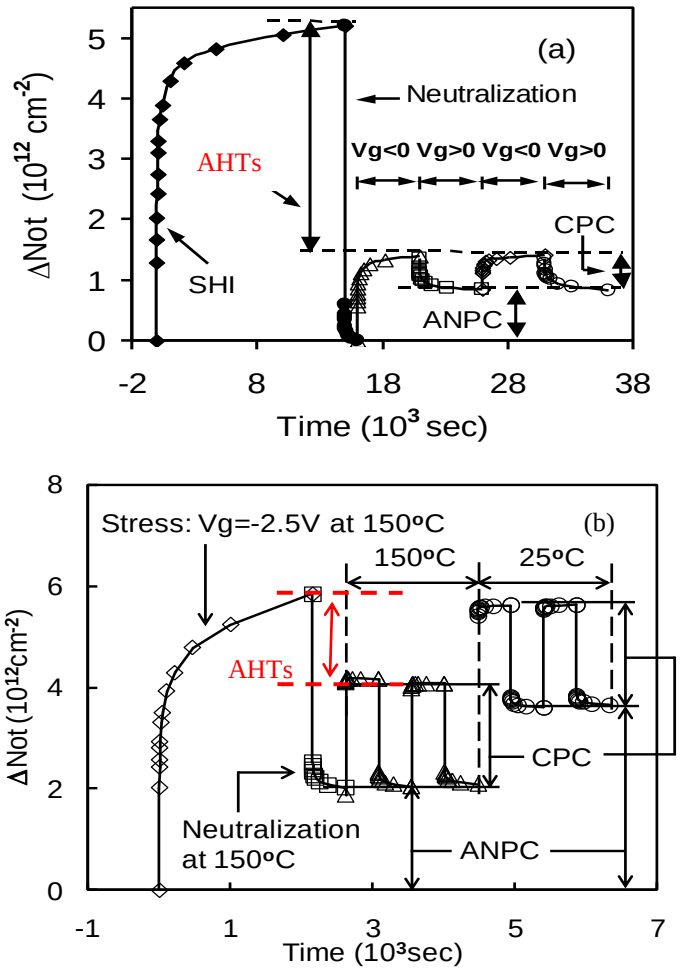

Fig. 13. A framework for positive charges in oxides: As-grown hole traps (AHTs); the generated Cyclic Positive Charges (CPC), and the generated Anti-Neutralization Positive Charges (ANPC). (a) After substrate hole injection [43, 44] and (b) after NBTI stress. [45]. ANPC are above Si Ec (see Fig. 14(a)) and require electrons above Ec for neutralization. Lowering temperature reduces electron above Ec and is less effective in neutralizing ANPC, resulting in the increase of ANPC when switching from 150 °C to 25 °C in (b).

In summary, the differences in charge-discharge properties of the three types of traps are: ANPCs can be easily charged, but difficult to neutralize; CPCs can both charge and discharge readily under relatively low oxide fields; and AHTs are most difficult to charge, but easy to discharge.

Although AHTs are most difficult to charge, they can dominate the charging during initial stress, because GDs are not generated yet, as shown in Fig. 11.

It should be pointed out that this framework was proposed based on test results of relatively thick (5.5 nm) oxide subjected to substrate hole injection [43,44]. For thin oxides stressed by NBTI, Fig. 13(b) shows that positive charges behave similarly, so that the same framework is applicable [45]. This framework is strongly supported by the energy profile of defects, as detailed below.

Based on their charge-discharge properties, the expected energy locations of the three kinds of positive charges are illustrated in Fig. 14(a). Like interface states, CPCs can cycle their charges when alternating gate bias polarity, so that their energy should be within Si bandgap. ANPCs are more difficult to neutralize than CPC and should stay above Si Ec. In contrast, AHTs are more difficult to charge than CPCs and should be located below Si Ev.

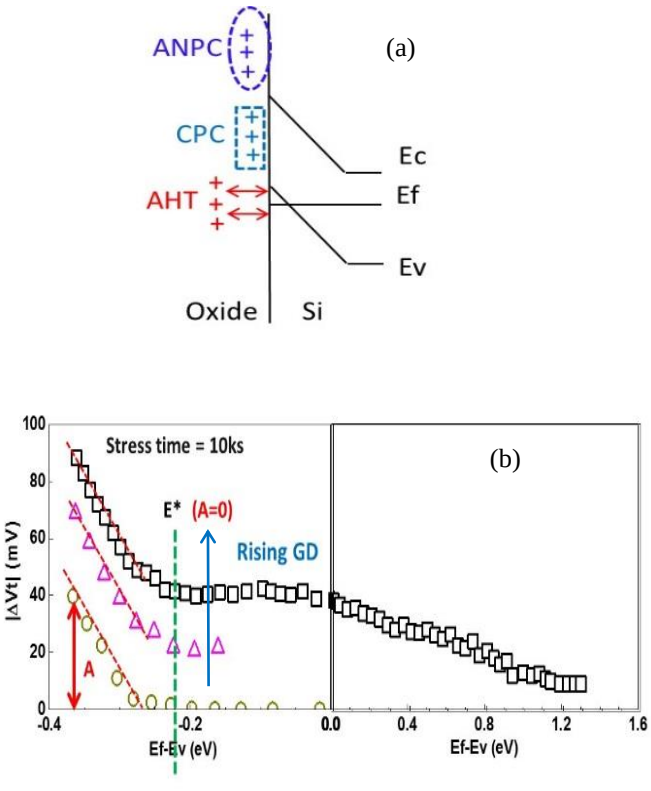

Fig. 14 Schematic (a) and measured (b) energy profile of positive charges in oxides. [28].

The energy profile illustrated in Fig. 14(a) is confirmed by measurements from the discharge-based technique detailed in [23]. The symbols 'o' in Fig. 14(b) show that after a short stress, all charges are located below E* (<Ev). Further stresses increase the charges above E*, but the charges below E* remain the same, as shown by the parallel shift of dashed lines in Fig. 14(b). This independence of stress strongly supports the 'as-grown' nature of hole traps below E*. In addition, Fig. 15 shows that the energy profile below Ev is independent of the energy-sweeping direction [46]. This confirms that the energy level of AHTs does not change with their charge status, as such a change should lead to hysteresis when sweeping in different directions.

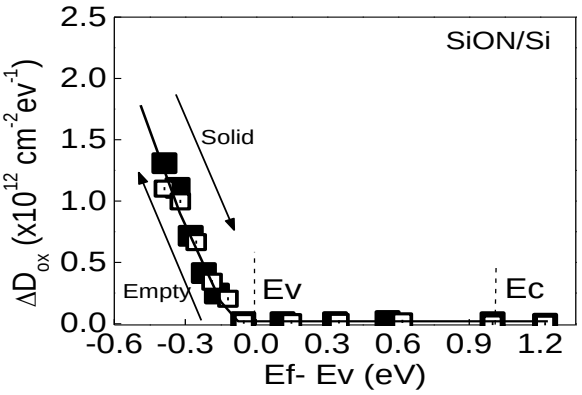

Fig. 15. Energy profile of AHTs does not depend on sweeping direction, so that energy level does not change with charge status. [46].

Although AHTs are most difficult to fill, the clear flat region in Fig. 16 shows that filling during stress is a rapid process, since it only takes a few milliseconds for a carrier to tunnel through a 2 nm SiON and reach traps within it, as shown in Fig. 17 [47]. If CPCs and ANPCs were present in a fresh device, they also should be charged, but Fig. 15 shows that there is no charges above Si Ev in a fresh SiON, supporting that they are generated. Fig. 14(b) confirms that stress increases positive charges both within the Si bandgap (CPC) and above Si Ec (ANPC). The step-like 'fast' charging-discharging behavior of CPCs and ANPCs in Fig. 13(b) also support that they are not traps of small capture cross sections.

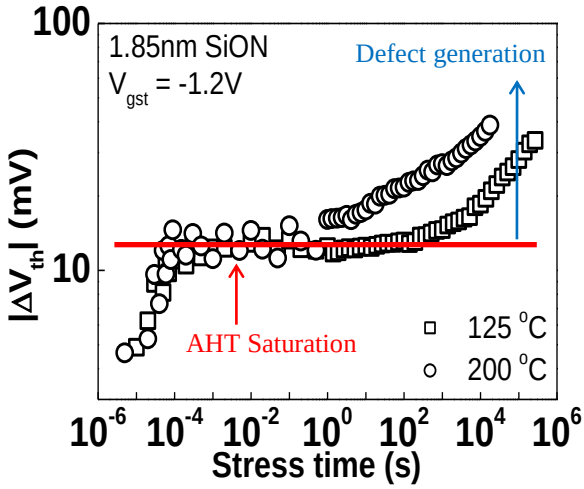

Fig. 16. AHTs dominate initially and reach saturation. The generated defects build up for longer stress time. [24].

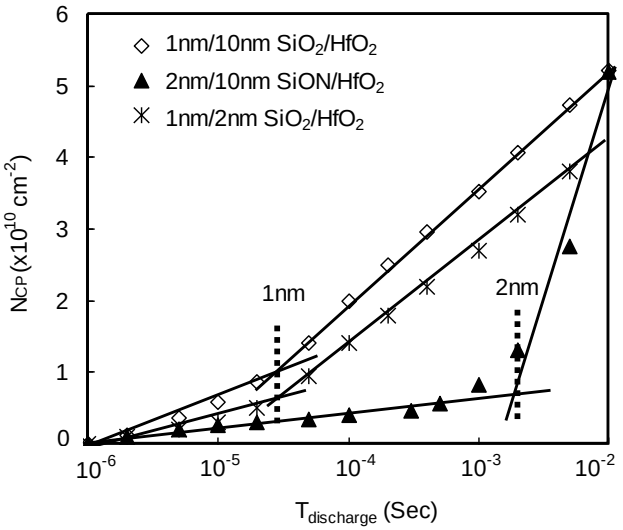

Fig. 17. Charge pumping at different discharge/recombination time. The dotted lines marks the transition from interfacial to high-k layers. [47].

The post-2000 works have used the terms of 'recoverable' and 'permanent' components [13,14] and their link with our framework should be clarified. AHTs only contribute to the recoverable component. CPCs also contribute to recoverable, as they are within Si bandgap. This is to say that recovery contains more than one kind of defects, including some generated defects. ANPCs dominate the permanent components. The so-called 'permanent' component actually can be neutralized. For example, the last '•' point in Fig. 13(a) reaches zero under high Eox>0 and ANPC is clearly lower when measured under higher temperature in Fig. 13(b). As a result, we consider that the term 'anti-neutralization' describes the defect better than 'permanent'.

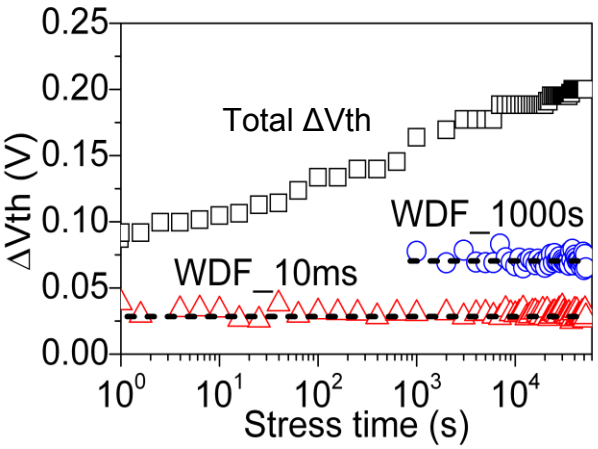

Fig. 18. Within-a-device-fluctuations (WDF), i.e. the RTN of multiple (>3) traps, measured with a fixed time window of 10 ms or 1000 sec do not change with stress levels. [48].

It is also worth of linking the framework with Random Telegraph Noise (RTN). RTN should be dominated by defects close to the Fermi-level, Ef, at the interface, as an occupancy around 0.5 leads to frequent charging-discharging events. This means that RTN is dominated by AHTs, since their energy level is close to Ef for typical RTN measurements, as shown in Fig. 14(a). As expected, Fig. 18 shows that the within-a-device-fluctuation (WDF), which is the RTN with more than 3~4 traps, is insensitive to NBTI stress time for a fixed measurement window [48].

3.4. Techniques for separating GDs from AHTs

An accurate separation of GDs from AHTs is important. Fig. 19 shows that a variation in estimated saturation levels of AHTs leads to different time exponents for GDs, making the long term prediction through extrapolation unreliable. Although the framework was proposed for the first time based on the charge-discharge properties given in Fig. 13, they cannot be used to give an accurate separation, as CPC levels depend on the magnitude of the alternating Eox used for their measurements. There are two other ways for separating GDs from AHTs: from NBTI kinetics and from energy profile.

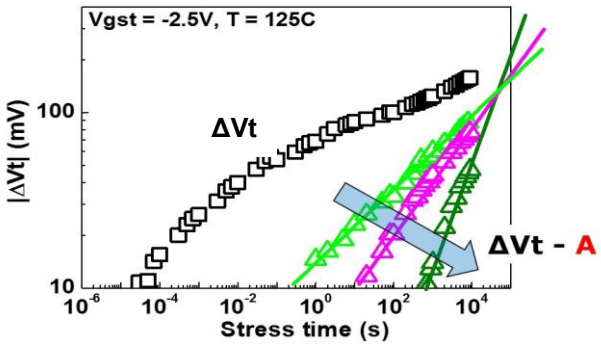

Fig. 19. After subtracting different amount of AHTs, **A**, all three sets of data apparently follow power law, but with different exponents.

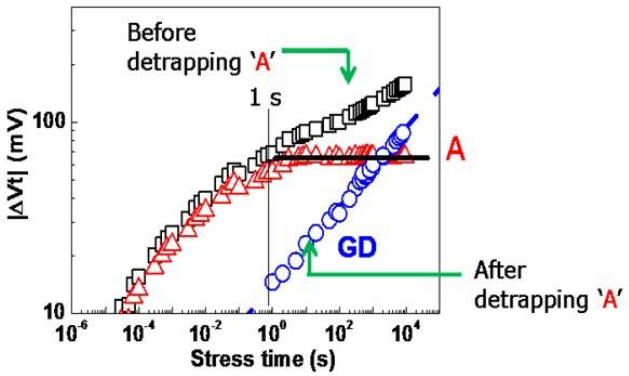

Fig. 20. Separation of GDs from AHTs, based on their different energy locations. AHTs remain saturated over four orders of stress time after 1 sec. [28].

To use NBTI kinetics for the separation, one must ensure that there are an initial period where NBTI is dominated by filling AHTs. This can be the case when stress bias is sufficiently low

that AHT-filling already completes before GDs become observable [21]. For higher biases typically used in accelerated NBTI stresses, filling AHTs for some samples also completes before GD becomes observable, as shown by the flat region in Fig. 16 [24]. In this case, the saturation level of AHTs can be directly measured from this flat level. For most samples under accelerated stresses, however, Figs. 5 and 19 show that such a flat region cannot be clearly observed, so that AHTs cannot be accurately separated from GDs in this way.

A general method for separating AHTs from GDs is based as their different energy locations: AHTs are below E*≤Ev and GDs are above it, as shown in Fig. 14(b). GDs can be measured at the energy level E*, therefore. An example of the separation is given in Fig. 20 for the case that NBTI kinetics does not have a clear flat region [28]. The GDs were measured directly from energy profile at E* and they follow a power law well. AHTs were then obtained by subtracting GDs from the total ΔVth. Fig. 20 shows that AHTs clearly dominates NBTI initially, but saturates around 1 sec. It is important to point out AHTs remain saturated in the following four orders of magnitude in stress time, confirming that they are 'as-grown'.

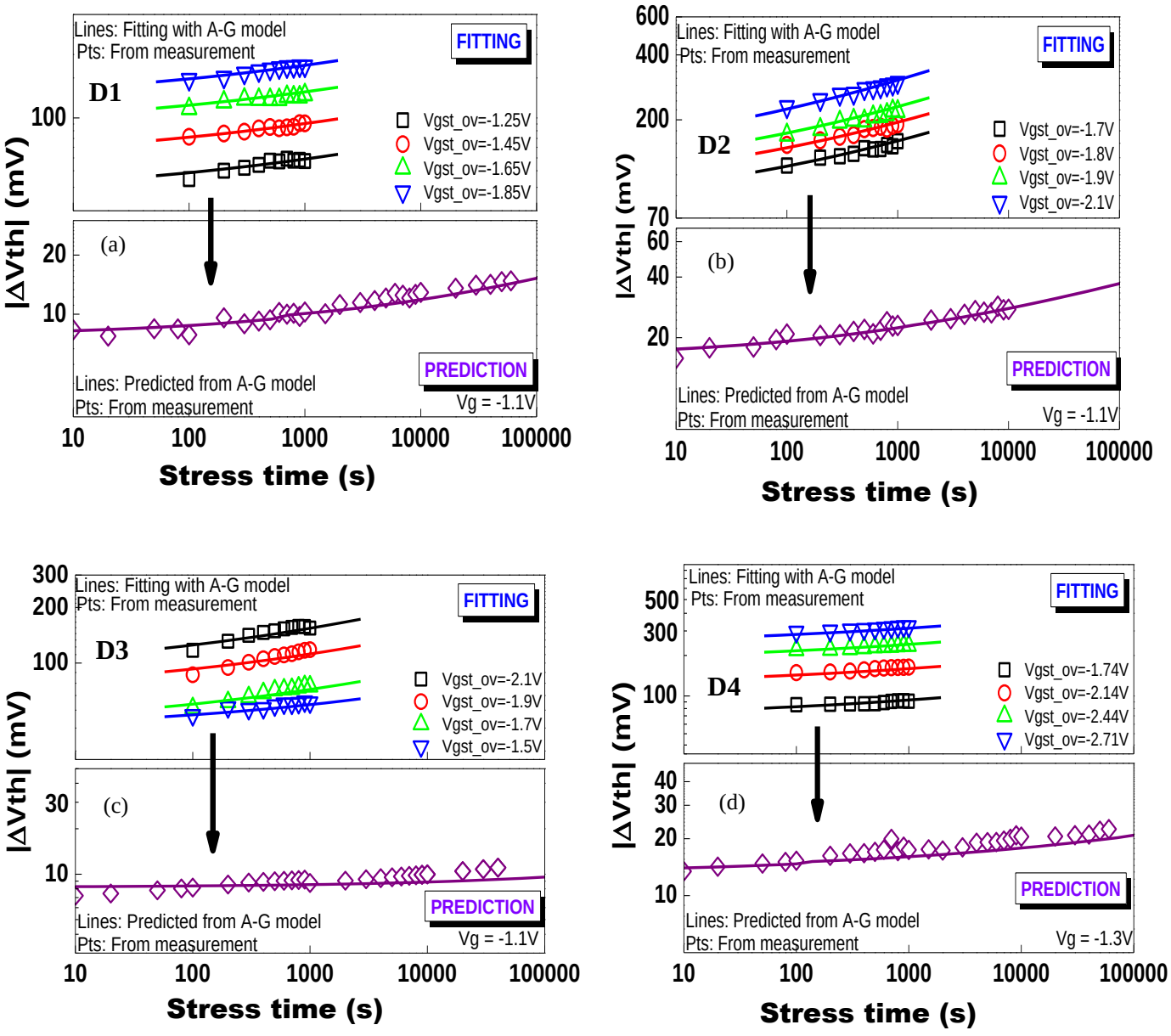

Fig. 21. Predictive capability assessment of AG model. The test data (symbols) are the same as that used for testing RD framework in Fig. 8. The lines in the upper panels are fitted with AG model. The lines in the lower panels are the prediction by the extracted model. The symbols in the lower panels are test data that were not used to fit the model parameters.

3.5. Prediction capability of AG model

The same data for testing the prediction capability of RD framework in Fig. 8 were used for testing AG model given below [28,29]:

$$\Delta Vth = AHT + gV_{gst}^{m}t^{n}. \quad (7)$$

As AHTs saturate within seconds, they can be evaluated from measurements and there is no need to predict them. In contrast, GDs follow a power law and do not saturate, so that prediction for the long term ageing is essential here.

The short and accelerated tests in the upper panels of Figs. 21(a)-(d) were used to extract the model parameters, g, m, and n. Unlike RD framework, the extracted AG model can predict the NBTI ageing at low biases well, as shown in the lower panels of Figs. 21(a)-(d).

3.6. An analysis of the prediction success of AG model

Like AG model, both RD framework and the composite models use a power law for part of NBTI: RD framework assumes that the creation of interface states follows a power law [7] and the composite model assumes that 'permanent component' follows a power law [13,14]. The question is why AG model can predict, while others cannot.

The composite model assumes that recoverable component increases with stress time without saturation [13]. For one set of test data, i.e. the measured ΔVth versus stress time, it fits two non-saturation kinetics. We found that this makes the extraction of time exponent unreliable. Even if one measures the 'recoverable' and 'permanent' component separately, the time exponent for the 'permanent' component will depend on the time and biases applied preceding the measurement of the 'permanent' component generally and one example is given in Fig. 3 [21]. It should also be pointed out that AHTs can dominate the recovery and their filling kinetics in Fig. 20 clearly saturates, in disagreement with the logarithmic time dependence of recoverable component, assumed by the composite model [13].

RD framework sets time exponent at 1/6 for the creation of interface states, based on the assumption that H_2 diffusion through oxides controls the generation [6,7]. At a typical work temperature of 125 °C, however, there is a lack of evidence that H_2 can react with interface states. Indeed, industry typically uses 350~400 °C for annealing interface states in forming gas that is a fixture of H_2 and N_2.

With a fixed time exponent of 1/6 for interface state generation, RD framework [7] extracts other model parameters for generated interface states, as-grown hole traps, and new hole traps from the same sets of test data, i.e. ΔVth versus stress time and biases. The formula used for these three components are different and we found that this is problematic. When we used different trapping kinetics, such as the one in the Composite model, the same test data can be fitted well.

Unlike RD framework and the composite models, AG model only fits one formulae, i.e. the power law of Eq.(7), with one set of data, as shown by the 'GD' in Fig. 20. AHTs and GDs are separated experimentally. Since AHTs saturate rapidly, they are evaluated from test data and we do not fit them. We believe that the simplified fitting of the experimentally evaluated GDs only with a power law allows parameters being reliably extracted and in turn gives the prediction capability.

For the pre-2000 NBTI works, lack of holes passing through oxides leads to negligible filling of AHTs, so that AHTs contributes little to their NBTI and the kinetics already follows power law. In contrast, the substantial hole injection into oxides for post-2000 works fills up AHTs and they can contribute considerably to NBTI, as shown in Fig. 20. Since AHTs are 'as-grown' and saturate rapidly, they do not result from long term ageing process. Their contamination of the real ageing power law must be removed. After this removal, GDs follow a power law well and behave like the pre-2000 works.

4. Mechanism and defects

The authors' works are based on electrical measurements and they do not give direct evidences on physical processes and atomic structures of defects. With this in mind, some speculations can be made on mechanism, defects, and damaging species, to improve understanding and to inspire further works in this area.

On the species causing ageing, two have been proposed: holes [33,49] and hydrogen [50]. Here 'holes' and 'hydrogen' refer to mobile species, rather than the immobile 'trapped holes' and 'hydrogen-bond'. For simplicity, 'hydrogen' here means 'hydrogenous species'.

Although the number of electrons injected into gate oxides is typically much higher than other species during stresses, it is considered that they do not cause ageing directly, but release either holes, hydrogen, or both. In 1990s, there were debates on the relative importance of these two [49,50], but this largely depends on their relative concentration during stress [51]. Most of these early works were not carried out under classical NBTI stress conditions. Some of them were not applicable to NBTI, but others can throw light on NBTI and help ruling out some possibilities. In this section, works on holes, hydrogen, and their interactions were briefly reviewed, before discussing their relevance to NBTI.

4.1. Holes

A number of ways have been proposed for holes to cause ageing:

- When a trapped hole captures an electron, the energy released from their recombination could cause damage [52].
- A two-stage process: a near interfacial hole trap captures a hole first. After neutralization, the structure relaxes and forms an interface state [53].
- Like electrons, holes can release hydrogen species, when they pass through the oxide [50]. This suggests that holes do not cause damage directly.

- The mobility of holes through oxides is extremely low, about six orders of magnitude smaller than that of electrons [54]. This heavy movement causes damage [33].
- Some hole traps can contain hydrogen species [51,55,56]. After capturing a hole and then neutralized, the hydrogen bond can be weakened and a hydrogen is released in oxides. When the hydrogen arrives at the interface, it reacts with Si-H and generates interface states, as shown in Fig. 22 [56]. This mechanism has been used to explain the delayed interface state generation post-hole injection [51,55]: After hole injection under Vg<0 terminates, interface states build up continuously, rather than recover, under Vg>0, as shown in Fig. 23 [55]. As a one-to-one correlation between generated interface state and GD has been observed [1-3], GD-precursors could be involved in the reaction.

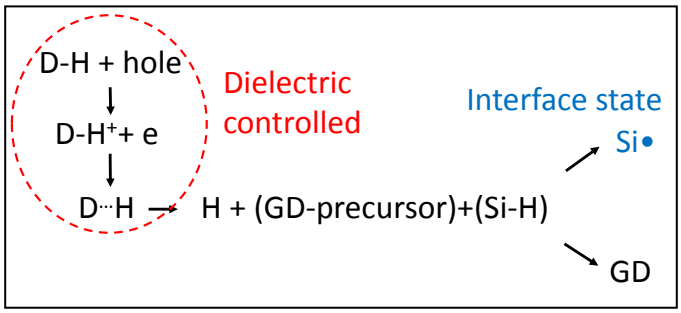

Fig. 22. A potential dielectric controlled process: Following hole trapping and neutralization, H is released from the weakened D···H, moves to interface, and creates interface states and GD. [56].

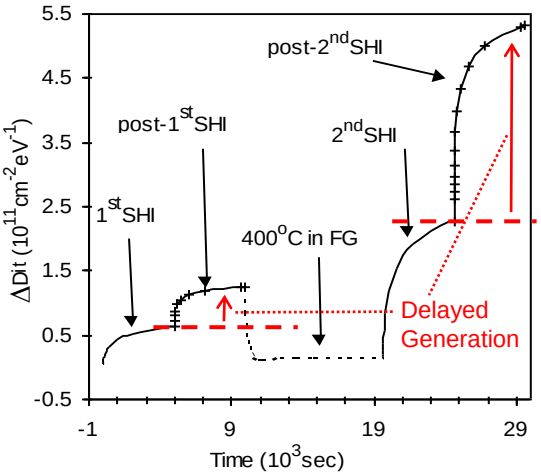

Fig. 23. A typical delayed interface state generation post-substrate hole injection. An increase of hydrogen after FG anneal enhances the generation. [55].

4.2. Hydrogen

Hydrogen can exist in oxides in different forms and interact with oxides in complex ways:

- H_2: As mentioned early, there is little evidence that H_2 can interact with oxides effectively at 125 °C or lower. Above ~350 °C, however, H_2 can be cracked by a Pb-centre and passivates interface states by forming Pb-H, which is a well-known industrial anneal process.
- Atomic hydrogen: Unlike H_2, H is highly reactive even at room temperature. At the interface, the reaction in Fig. 24 is bi-directional. At 400 °C, it moves from left to right, annealing interface states. At room temperature, however, the annealed interface states are regenerated by an exposure to H, as shown in Fig. 25 [57]. This agrees with the assumption that the hydrogen released during electrical stresses at room temperature creates interface states, rather than passivating them [50].
- Protons: hydrogen can also exist as H^+. Like H, H^+ is also reactive at room temperature. H^+ can be formed in oxides during irradiation [58]. They can then be driven to the interface under Vg>0 and cause a delayed generation of interface states post-irradiation [58]. It has been reported that proton gives a time exponent of 0.5 [4].
- Inactive hydrogenous species: hydrogen can also exist in other forms in oxides and one of them is inactive hydrogen. At ~500 °C or lower, Si-H bond is thermally stable. Above this temperature, Si-H dissociates [59]. This, however, does not mean hydrogen cannot stay in oxides stably. When annealed at temperature over 500 °C in H_2, both mobile and fixed positive hydrogenous species are formed [60]. These mobile positive charges can be cycled between the gate and Si by alternating gate bias polarity, as shown in Fig. 26. It should be noted that under Vg>0, positive charges move to the interface and increase the effective charge density, opposite to the recovery of NBTI under Vg>0 in Fig. 13. Unlike H and H^+, however, they do not react at the interface and does not create interface states. The atomic structure of these inactive hydrogenous species is not known. Since H^+ and H are highly reactive and Si-H is unstable above 500 °C, one may speculate that oxygen is involved in some way.

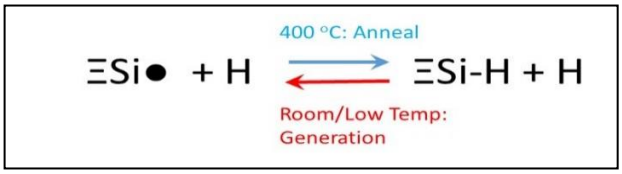

Fig. 24. The bi-directional reaction between atomic hydrogen, H, and interface state precursor.

4.3. Interaction between holes and hydrogen

Both holes and hydrogen can cause damage independently, but they also can interact. To show this interaction, the test procedure in Fig. 27(a) was used: After stress and filling hole traps to the point 'A', the device was exposed to H_2 at 400 °C to reach the point 'B' [51]. The stress and filling were then resumed up to the point 'C'. The following observations can be made:

- Although neutral hole traps do not react with H_2, a trapped hole can crack H_2 in Fig. 28. To support this, Fig. 29 shows that the neutralization in a relatively thick (7 nm) oxide proceeds linearly against logarithmic time in N_2 at 400 °C, but clearly accelerates in the presence of mobile H_2 [61].

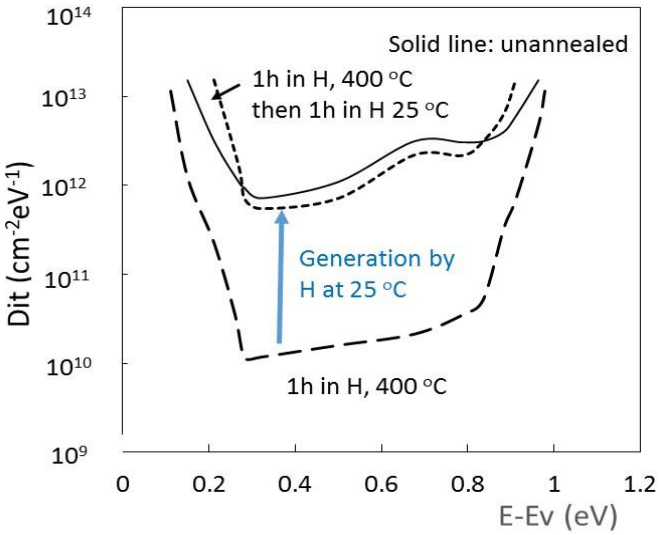

Fig. 25. The device was exposed first to atomic hydrogen, H, at 400 °C for 1 hour and the interface states were annealed. It was then exposed to H at 25 °C for another hour, during which the annealed interface states were re-generated. [57].

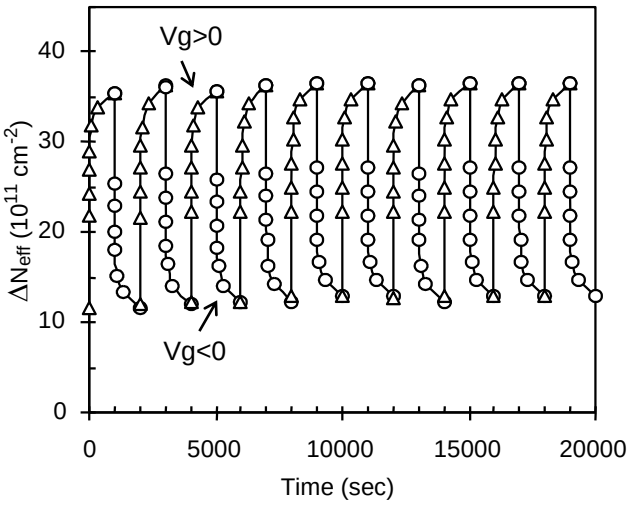

Fig. 26. Formation of inactive and mobile positive hydrogenous species after exposure to H_2 at ≥ 500 °C. [60].

- The released H^+ moves through oxides and creates CPCs. Fig. 30 shows that an increase of the interaction leads to a higher level of CPCs at the start of subsequent hole injection because there are more neutral CPCs available for filling. As stress increases, CPCs saturate at the same level in all three cases, confirming that there is a limited CPC precursors for the generation.

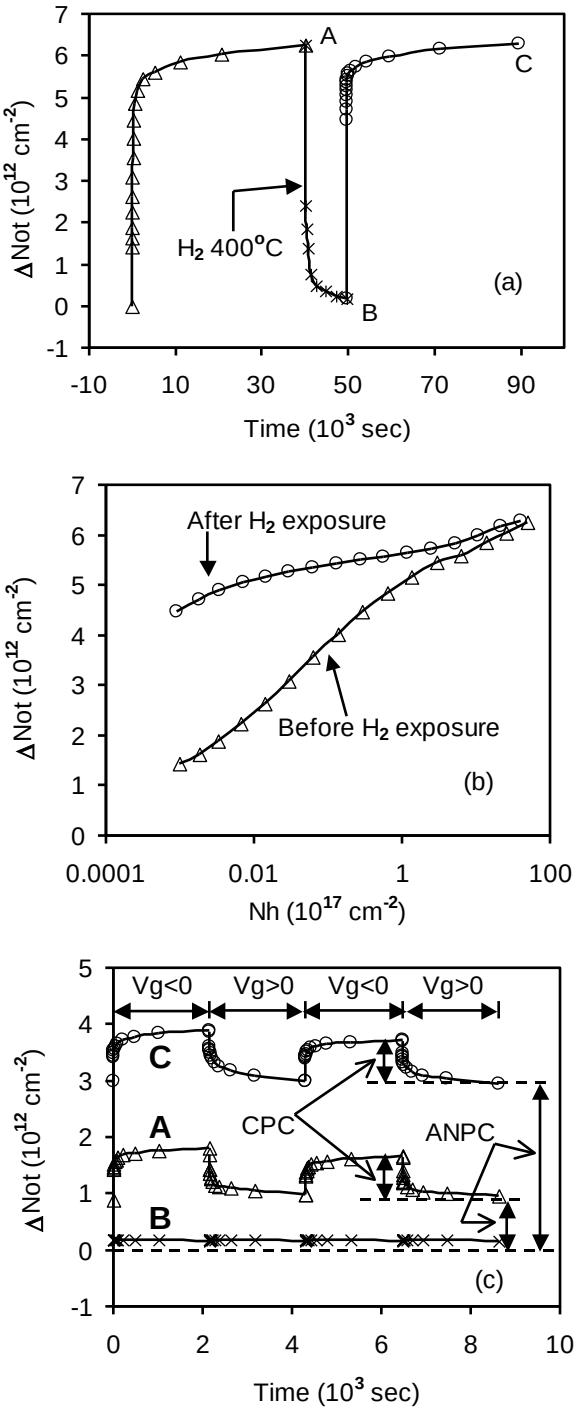

Fig. 27. Interaction between hole traps and hydrogen. (a) After the 1st hole injection, trapped holes were neutralized in H_2 at 400 °C, followed by the 2nd hole injection. (b) A comparison of the trapping for the 1st and 2nd injection. (c) CPCs and ANPCs at the point A, B, and C in (a). [51].

The H_2 were cracked at 400 °C here, but a chip typically will not be exposed to such a high temperature after fabrication. The device, however, is commonly exposed to hydrogen during the fabrication. Fig. 31 shows that, for a process under development, the hydrogen during the fabrication converted all CPC-precursors, so that CPCs saturates at the first test point already.

$$\text{(hole trap)} + \text{hole} \rightarrow \text{(hole trap)}^+$$

Crack

$$\text{(hole trap)}^+ + H_2 \rightarrow \text{(hole trap)-H} + H^+$$

$$\text{(hole trap)-H} + \text{hole} \rightarrow \text{(hole trap)-H}^+$$

Fig. 28. Interaction of hole traps with H_2. [51].

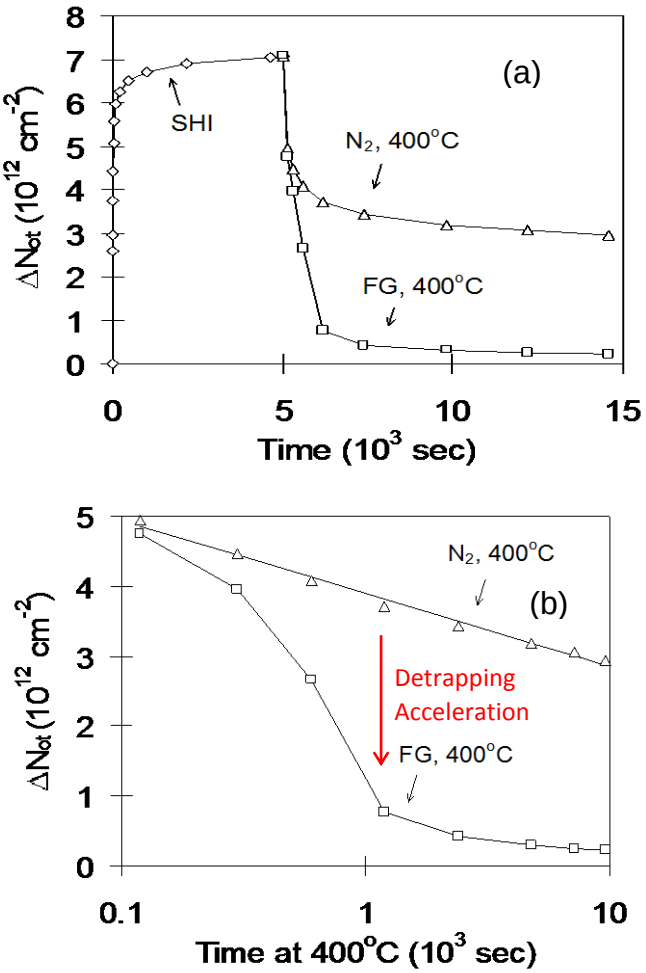

Fig. 29. (a) A comparison of neutralization in N_2 and Forming Gas (FG). (b) Detrapping follows logarithmic time linearly in N_2, but accelerates in FG. [61].

- The impact of the interaction on ANPC is given in Fig. 32. After the interaction, the first point jumped up, but subsequent generation is hardly affected.
- The initial jump in the apparent ANPC in Fig. 32 results from hydrogenation of AHT to form AHT-H. As the total trapping level at the point 'A' and 'C' in Fig. 27(a) is the same and with CPC saturates at the same level, an increase of ANPC must have a corresponding reduction of AHTs. Fig. 28 illustrates that AHT-H bond can be formed and when capturing a hole, the AHT-H^+ is more difficult to neutralize than that before hydrogenation, most likely because the energy level of AHT-H^+ moves above Si Ec [51].

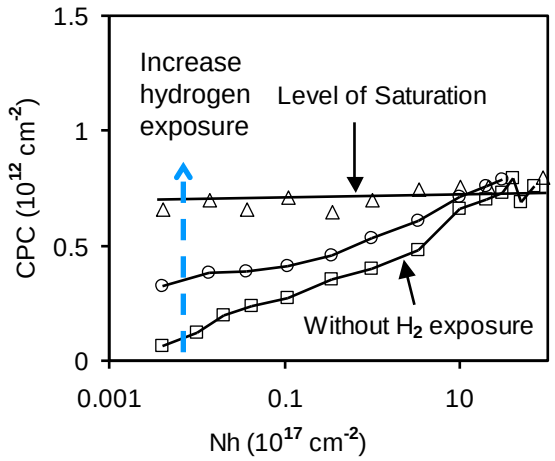

Fig. 30. Impact of hydrogenation on the generation of CPCs. [51].

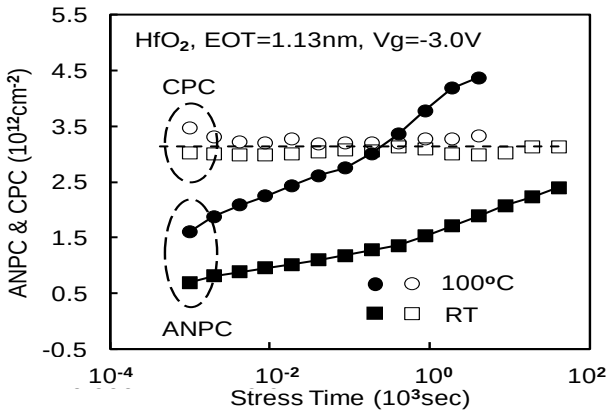

Fig. 31. Generation of CPCs by hydrogenation during fabrication leads to CPC reaching saturation at the first test point. [45]

To support the formation of AHT-H^+, we cycled the stress/H_2-anneal and stress/N_2-anneal. Fig. 33 shows that this apparent ANPC can be partially removed after N_2-anneal by driving out the H^+ introduced through H_2-anneal. After exposing to H_2 again, the removed apparent ANPC returned.

As mentioned earlier, AHTs dominate RTN. Once AHT-H^+ are formed, they are difficult to neutralize and may lead to the 'loss of RTN signal'. As AHT-H^+ is not stable, the RTN signal can reappear. This may contribute to the temporary passivation-reactivation of RTN signals [62].

4.4. Defects and Mechanism of NBTI

As-grown hole traps: As mentioned early, the main difference between pre- and post-2000 NBTI works are the charging AHTs by hole transporting through the dielectric in the latter. Higher |Vg| allows AHTs further below Si Ev being charged, as shown in Figs. 14(b) and 15 [28,46]. They can dominate the post-2000 NBTI initially, but saturate generally within seconds. After NBTI stresses, neutralization of trapped holes has not led to a corresponding generation of interface states, so that neither the energy released by recombination [52] nor the structure relaxation following AHT-neutralization [53] are important [63].

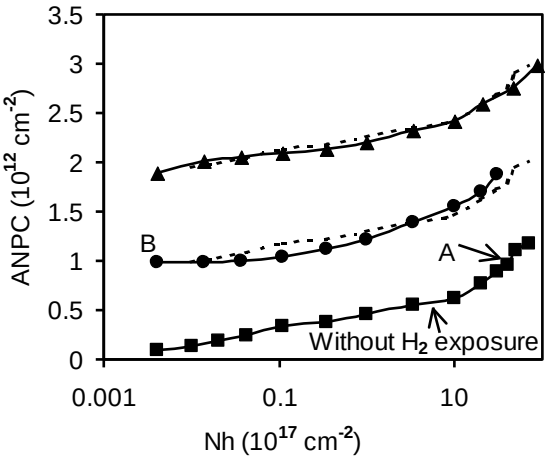

Fig. 32. Impact of hydrogenation on the generation of ANPCs. The two dashed curves were a parallel up-shift of the lowest curve [51].

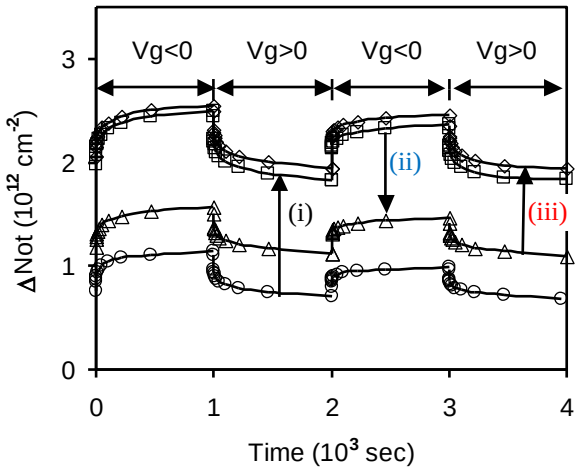

Fig. 33. Impact of the hydrogen density on the apparent ANPC: (i) H_2 exposure raised it; (ii) N_2 exposure reduces it; and (iii) The 2nd H_2 exposure raises it again. [51].

AHTs pile up towards the oxide/Si interface [64] and most likely originate from oxygen vacancies (Vo) [65] or strained Si-O bonds [53,66]. Their effective density can reach 10^{13}cm^{-2} [35], about one order of magnitude higher than that of Pb [59]. Their energy level generally is below Si Ev and does not change after charging-discharging, as shown in Fig. 15 [46].

By cracking H_2 at 400 °C, AHT-H^+ can be formed, which enhances the post-stress generation in Fig. 23 through the mechanism in Fig. 22. For the post-2000 NBTI, this mechanism could contribute, as both electrons and holes were injected into oxides during stress, enabling the reaction in Fig. 22. If such a process is important, one would expect that after terminating NBTI stress, the continuing hydrogen-release would keep interface state building up for some time [56]. This delayed generation is, however, not observed after typical NBTI stress, probably because there is little AHT-H available in modern thin oxides. The positive AHTs in thin oxides can be neutralized efficiently by tunneling and neutral AHTs do not react with H_2. Indeed, Fig. 14(b) shows that AHTs are hardly affected by the stress for thin oxides. As a result, the main effect of AHTs on NBTI is a straightforward charge-discharge, which is independent of defect generation.

The potential candidates for AHTs must meet these conditions: An energy level below Si Ev; Charge-discharge without changing energy level; Pile-up towards interface with a high density of 10^{13}cm^{-2}; Can exist as AHT, AHT$^+$, AHT-H, and AHT-H$^+$; AHT-H$^+$ is hard to neutralize than AHT$^+$.

Cyclic positive charges (CPC): The number of CPC-precursors is clearly limited. Whether the original CPC-precursors contain hydrogen is not known, but they must be able to react with mobile H/H$^+$. After 400 °C exposure in H_2, CPC appears passivated, most likely by forming some hydrogen bonds, CPC-H. This passivation, however, is different from the passivation of interface states by forming Pb-H: The CPC-H is not the same as CPC-precursor. Like AHTs, CPC-H becomes fully charged at the first point in Figs. 30 and 31 and there is no longer a generation process needed here. As CPC-Hs are not CPC-precursors, one may speculate that CPC-precursors do not contain a hydrogen bond, unless somehow CPC-precursors can contain a different type of hydrogen bond. When considering their potential microscopic structure for CPCs, the followings should be taken into account:

- The neutral CPC-precursors have a fixed number over one order of magnitude less than AHTs.
- Once generated, CPCs can be repeatedly charged and discharged with energy levels in Si bandgap.
- Both CPC-precursors and CPC can react with H$^+$/H to form neutral CPC-H that is different from the CPC-precursors.
- CPC-H are effective hole traps.

Anti-neutralization positive charge (ANPC): In contrast to CPCs, Fig. 32 shows the stress-induced ANPCs are not affected by the exposure to H_2 at 400 °C. This indicates that the precursors responsible for the stress-induced ANPCs have fully recovered to their initial status in a fresh device and the exposure did not increase their density. Like the anneal of interface states by forming Pb-H, ANPCs are probably annealed by re-forming ANPC-H at 400 °C. In another word, it is likely that ANPC-H is the ANPC precursor, containing a hydrogen-bond.

The assumption that ANPC-precursors contain hydrogen bond agrees with the observation of 'defect-loss' for the 'permanent components' [67,68]. After weakening ANPC-H through capturing a hole, an exposure to elevated temperature can drive some hydrogen away, leading to the loss.

As both CPC and ANPC are generated defects, one may ask whether they have the same atomic structure, just with different energy levels. Although this cannot be definitely ruled out, it does not agree with their contrasting behavior when exposed to H_2 at 400 ^oC in Figs. 30 and 32.

The atomistic candidates for ANPC must be able to: fully anneal in H_2 at 400 ^oC; Have energy levels above Si Ec in both neutral and positive charged form; Be a hole trap; Have a structure that does not further relax following charge/discharge; Be different from AHTs.

The generation process: As mentioned earlier, if mobile hydrogen released from oxide bulk is important for the generation, one would expect that generation continues for some time after terminating NBTI stress. The post-stress generation is indeed observed following irradiation [58,69] and an increase of hydrogen in the oxide after hole injection clearly enhances the delayed generation in Fig. 23 [55,56]. After NBTI tests, however, recovery is typically reported, rather than a delayed post-stress generation, indicating hydrogen release from oxides is less important. The modern oxides also are too thin for hydrogen diffusion as the rate limiting process: For a 42 nm oxide, the transportation completes in ~ 1000 sec [69].

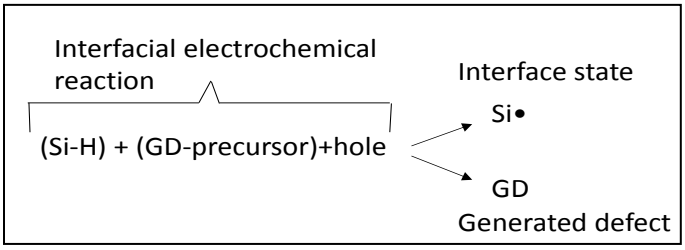

Fig. 34. Controlling the NBTI rate: a potential electrochemical reaction near the interface.

It is likely that defect generation for both pre- and post-2000 NBTI is controlled by the same electrochemical reaction near the interface and a potential candidate is given in Fig. 34 [3,4]: Holes are essential in this reaction, as there is little interface state generation when holes are kept away from the interface under positive gate bias [70]. Si-H at interface has been widely accepted as the interface state precursor. In case that Si-H is too strong to be broken by direct interaction with holes, a GD-precursor also could be involved in the reaction, catalyzing the rupture of Si-H. One may speculate that the rate limiting step is the rupture of Si-H. The amorphous nature of oxides means that there can be a distribution of bond-strength in the local network, giving rise to the empirical power law kinetics. To explain the one-to-one correlation between the number of generated interface states and positive oxide charges [1-3], one may speculate that Si-H and GD-precursor are linked in some way. The details, however, await further works.

5. Summary

This paper reviews NBTI modelling, defects, damaging species, and mechanism. In comparison with negligible hole injection into gate oxides in pre-2000 works, there are substantial hole injection in post-2000 works, because of the high field and thin oxide used. The injected holes fill up As-grown Hole Traps (AHTs) rapidly, adding a new component to NBTI. This causes a number of discrepancies with pre-2000 works: oxide charges can be higher than the number of generated interface states; recovery can be over 50%; and the kinetics is no longer a power law when recovery is suppressed. Although the models proposed by the post-2000 works can fit short accelerated test data well, evidences are not strong enough to convince that they generally can predict long term NBTI under use-Vdd and it has been shown that RD framework cannot predict. One reason for this failure is that the new AHT component has not been accurately separated from others. AHTs contaminate the real NBTI ageing kinetics and induce errors in the extracted model parameters.

A framework for positive charges in oxides has been proposed: AHTs are below Si Ev, hard to charge, and easy to neutralize; Cyclic Positive Charges (CPCs) are within Si bandgap and their charge cycles with gate polarity; Anti-Neutralization Positive Charges (ANPCs) are above Si Ec, easy to charge, but hard to neutralize. Both CPCs and ANPCs are Generated Defects (GDs). Based on this framework, the As-grown-Generation (AG) model is developed. GDs are successfully separated from AHTs and only GDs follow the power law, similar to pre-2000 works. The prediction capability of AG model is demonstrated.

Although the electrical test results given in this work do not offer direct evidences for atomistic structures of the defects and ageing mechanism, some speculations were made. The hydrogenous species, holes, and their interactions play essential roles in NBTI. The conditions that potential candidates must meet for AHTs, CPCs, and ANPCs are discussed. Physical processes in oxides, such as hydrogen transportation and emission, generally lead to delayed build-up of interface states, which is rarely observed in typical NBTI tests. As a result, in addition to filling AHTs, NBTI ageing rate is likely controlled by an electrochemical reaction near the interface with a widely spread rate giving rise to the power law kinetics.

Acknowledgements

This work is based on long collaboration with IMEC, Belgium, and we acknowledge valuable discussions with IMEC colleagues who supplied most of test samples used in this work. The contributions of PhD students and post-doctoral research fellows at Liverpool John Moores University make this work possible. We thank Prof Grasser at TU Wien for useful discussions. The work is supported by the EPSRC of UK under the grant nos. GR/L28531, GR/R10387/01, EP/C003071/1, EP/I012966/1, and EP/L010607/1.

REFERENCES

[1] Deal BE, Sklar M, Grove AS, Snow EH. J Electrochem Soc 1967; 114:266
[2] Jepson KO, Svensson CM. J Appl Phys 1977; 48:2004.
[3] Blat CE, Nicollian EH, Poindexter EH. J Appl Phys 1991; 69:1712.
[4] Ogawa S, Shimaya M, Shiono N. J Appl Phys 1995; 77:1137.
[5] Kimizuka N et al. In: Proceeding of Symp VLSI Tech, 1999. p. 73.
[6] Joshi K et al. In: Proceedings of the International Reliability Physics Symposium, 2012. p. 5A.3.1.
[7] Mahapatra S et al. IEEE Trans Elec Dev 2013; 60:901.
[8] Kaczer B et al. In: Proceedings of the International Reliability Physics Symposium, 2010. p. 26.
[9] Stathis JH, Zafar S. Microelectronics Rel 2006; 46:270.
[10] Grasser T et al. IEEE Trans Elec Dev 2011; 58:3652.
[11] Grasser T et al. In: Proceedings of the International Reliability Physics Symposium, 2010. p. 16.
[12] Grasser T et al. In: Proceedings of International Electron Device Meeting, 2015. p. 535.
[13] Huard V. In: Proceedings of the International Reliability Physics Symposium, 2010. p. 33.
[14] Huard V et al. IEEE Trans Dev Materials 2007; 7:558.
[15] Teo ZQ, Ang DS, See KS. In: Proceeding of International Electron Device Meeting, 2008. p. 737.
[16] Reisinger H et al. In: Proceedings of the International Reliability Physics Symposium, 2006. p. 448.
[17] Kerber A, Krishnan SA, Cartier EA. IEEE Electron Device Lett 2009; 30:1347.
[18] Ren P et.al, In: Proceeding of International Electron Device Meeting, 2014. p. 816.
[19] Chang MH, Zhang JF. J Appl Phys 2007; 101:024516.
[20] Zhang JF. IEEE Electron Device Lett 2008; 29:1360.
[21] Gao R et.al. IEEE Trans Elec Dev 2017; 64:1467.
[22] Ji Z, Zhang JF, Chang MH, Kaczer B, Groeseneken G. IEEE Trans Elec Dev 2009; 56:1086.
[23] Hatta SFWM et al. IEEE Trans Elec Dev 2013; 60:1745.
[24] Ji Z, Lin L, Zhang JF, Kaczer B, Groeseneken G. IEEE Trans Elec Dev 2010; 57:228.
[25] Hicks J et al. Intel Technology Journal, 2008; 12:131.
[26] Krishnan AT et al. In: Proceedings of International Electron Device Meeting, 2006.
[27] Lin L, Ji Z, Zhang JF, Zhang WD, Kaczer B, De Gendt S, Groeseneken G. IEEE Trans Elec Dev 2011; 58:1490.
[28] Ji Z et.al. In: Proceedings of International Electron Device Meeting, 2013. p. 413.
[29] Ji Z et al. In: Proceedings of Symp VLSI Tech, 2015. p. 36.
[30] DiMaria DJ, in The Physics of SiO_2 and Its Interfaces, Pergamon, New York, 1978. p. 160.
[31] Chang MH, Zhang JF, Zhang WD, IEEE Trans Elec Dev 2006; 53:1347.
[32] Young DR. Inst Phys Conf Ser 1980; 50:28.
[33] Zhang JF, Taylor S, Eccleston W. J Appl Phys 1992; 71:725.
[34] Wolters DR van der Schoot JJ. J Appl Phys 1985; 58:831.
[35] Zhang JF, Sii HK, Groeseneken G, Degraeve R. IEEE Trans Elec Dev 2001; 48:1127.
[36] Zhang WD, Zhang JF, Lalor M, Burton D, Groeseneken G, Degraeve R. IEEE Trans Elec Dev 2002; 49:1868.
[37] Zhang JF et al. Semiconductor Sci. and Technology 2004; 19:L1.
[38] Hu C et al. IEEE Trans Elec Dev 1985; ED-32:375.
[39] Stathis JH, DiMaria DJ, In: Proceeding of International Electron Device Meeting, 1998. p. 167.
[40] Stathis JH, DiMaria DJ. Microelectronic Eng 1999; 48:395.
[41] Zhang WD, Zhang JF, Zhao CZ, Chang MH, Groeseneken G, Degraeve R. IEEE Electron Device Lett 2006; 27:393.
[42] Zhao CZ, Zahid MB, Zhang JF, Groeseneken G, Degraeve R, De Gendt S. Zhao, Microelectronic Eng 2005; 80:366.
[43] Zhang JF, Zhao CZ, Chen AH, Groeseneken G, Degraeve R. IEEE Trans Elec Dev 2004; 51:1267.
[44] Zhao CZ, Zhang JF, Groeseneken G, Degraeve R. IEEE Trans Elec Dev 2004; 51:1274.
[45] Zhao CZ, Zhang JF, Chang MH, Peaker AR, Hall S, Groeseneken G, Pantisano L, De Gendt S, Heyns M. IEEE Trans Elec Dev 2008; 55:1647.
[46] Ma J, Zhang W, Zhang JF, Benbakhti B, Ji Z, Mitard J, Arimura H. IEEE Trans Elec Dev 2016; 63:3830.
[47] Zheng XF, Zhang WD, Govoreanu B, Zhang JF, Van Houdt J. IEEE Trans Elec Dev 2010; 57:2484.
[48] Duan M et al. In: Proceedings of Symp VLSI Tech, 2014. p. 74.
[49] Bude JD, Weir BE, Silverman PJ. In: Proceedings of International Electron Device Meeting, 1998. p. 179.
[50] DiMaria DJ, Stathis JH. J Appl Phys 2001; 89:5015.
[51] Zhao CZ, Zhang JF. J Appl Phys 2005; 97:073703.
[52] Chen IC, Holland S, Hu C. J Appl Phys 1987; 61:4544.
[53] Lai SK. J Appl Phys 1983; 54:2540.
[54] Hughes RC. Phys Rev B 1977; 15:2012.
[55] Zhao CZ, Zhang JF, Groeseneken G, Degraeve R, Ellis JN, and Beech CD. J Appl Phys 2001. 90:328
[56] Zhang JF, Zhao CZ, Groeseneken G, Degraeve R, J Appl Phys 2003. 93:6107.
[57] Do Thanh L, Balk P. J Electrochem Soc 1988; 135:1797.
[58] Saks NS, Klein RB, Griscom DL. IEEE Trans Nuclear Science 1988; 35:1234.
[59] Stesmans A. Phys Rev B; 61:8393.
[60] Zhang JF, Zhao CZ, Groeseneken G, Degraeve R, Ellis JN, Beech CD. J Appl Phys 2001; 90:1911.
[61] Zhang JF, Zhao CZ, Groeseneken G, Degraeve R, Ellis JN, Beech CD. Solid-State Electronics 2002; 46:1839.
[62] Grasser T et al. In: Proceeding of International Electron Device Meeting, 2013. p. 409.
[63] Al-kofahi IS, Zhang JF, Groesenen G. J Appl Phys 1997; 81:2686.
[64] DiMaria DJ, Weinberg ZA, Aitken JM. J Appl Phys 1977; 48:898.
[65] W. L. Warren WL, Lenahan PM, J Appl Phys 1987; 62:4305.
[66] Grunthaner J, Lewis BF, Zamini N, Maserjian J, Madhukar A. IEEE Trans Nucl Sci 1980; NS-27:1640.
[67] Duan M, Zhang JF, Ji Z, Zhang W, Kaczer B, De Gendt S, Groeseneken G. IEEE Electron Device Lett 2012; 33:480.
[68] Duan M, Zhang JF, Ji Z, Zhang W, Kaczer B, De Gendt S, Groeseneken G. IEEE Trans Elec Dev 2013; 60:413.
[69] Saks NS, Brown DB. IEEE Trans Nuclear Science 1989; 36:1848. (42nm 1000 sec saturation approached)
[70] Duan M, Zhang JF, Ji Z, Zhang W, Vigar D, Asenov A, Gerrer L, Chandra V, Aitken R, Kaczer B. IEEE Trans Elec Dev 2016; 63:3642.